SANDIA REPORT

SAND2019-11190
Printed September, 2019

Sandia National Laboratories

Estimating Regional Methane Emissions Through Atmospheric Measurements and Inverse Modeling

Cosmin Safta, Ray Bambha, Hope Michelsen

Prepared by
Sandia National Laboratories
Albuquerque, New Mexico 87185
Livermore, California 94550

Issued by Sandia National Laboratories, operated for the United States Department of Energy by National Technology & Engineering Solutions of Sandia, LLC.

Available to DOE and DOE contractors from

U.S. Department of Energy
Office of Scientific and Technical Information
P.O. Box 62
Oak Ridge, TN 37831

Telephone: (865) 576-8401
Facsimile: (865) 576-5728
E-Mail: reports@osti.gov
Online ordering: http://www.osti.gov/scitech

Available to the public from

U.S. Department of Commerce
National Technical Information Service
5301 Shawnee Road
Alexandria, VA 22312

Telephone: (800) 553-6847
Facsimile: (703) 605-6900
E-Mail: orders@ntis.gov
Online order: https://classic.ntis.gov/help/order-methods

ABSTRACT

In this report we describe an enhanced methodology for performing stochastic Bayesian inversions of atmospheric trace gas inversions that allows the time variation of model parameters to be inferred. We use measurements of methane atmospheric mixing ratio made in Livermore, California along with atmospheric transport modeling and published prior estmates of emissions to estimate the regional emissions of methane and the temporal variations in inferred bias parameters. We compute Bayesian model evidence and continuous rank probability score to optimize the model with respect to temporal resolution. Using two different emissions inventories, we perform inversions for a series of models with increasing temporal resolution in the model bias representation. We show that temporal variation in the model bias can improve the model fit and can also increase the likelihood that the parameterization is appropriate, as measured by the Baysian model evidence. .

CONTENTS

LIST OF FIGURES

1. INTRODUCTION

The concentration of methane at the Earth's surface is believed to have increased by 150% since the pre-industrial years, and the contribution of methane to global radiative forcing is second only to carbon dioxide [18] among the greenhouse gases. A number of studies have found significantly greater emissions estimates in North America inferred from atmospheric measurements by comparison to those reported in inventories of methane emissions [17, 9, 11]. Although the aforementioned studies have provided valuable information on the deficiencies of methane emission estimates, greater detail on the spatial and sectoral distribution of emissions is needed to inform new policies and assess their effectiveness. In order to reduce the uncertainty in the emissions estimates from top-down studies it will be important to understand the relative contributions of different sources of uncertainty. The application of hierarchical Bayesian methods to atmospheric trace gas inversions has allowed the uncertainty in parameters used in inversions to be inferred [4, 11]. In previous studies the model discrepancies have been considered constant over months or seasons. The study presented here provides further development in the methodology for stochastic Bayesian inversion for trace gases to allow for much higher temporal fluctuations in the model discrepancies through the use of a random-field expansion in the multiplicative model bias. We performed our analysis over four months in 2015 for the San Francisco Bay region of California using methane measurements from a single measurement site and demonstrate a reduction in the uncertainty in monthly emissions estimates for the region for some months.

2. ACKNOWLEDGMENT

This works was supported by Laboratory Directed Research and Development program at Sandia National Laboratories. Sandia National Laboratories is a multimission laboratory managed and operated by National Technology & Engineering Solutions of Sandia, LLC, a wholly owned subsidiary of Honeywell International Inc., for the U.S. Department of Energy's National Nuclear Security Administration under contract DE-NA0003525. This report describes objective technical results and analysis. Any subjective views or opinions that might be expressed in the report do not necessarily represent the views of the U.S. Department of Energy or the United States Government.

3. PROBLEM SETUP

The time dependent CH_4 concentration $y(t,x_r)$ at time t and receptor location x_s (usually the location of the instrument) is modeled as

$$y(x_r,t) \approx b + \int_{t-\Delta t}^{t} \int_{\mathbb{A}} F(x,\tau;x_r,t)E(x,\tau)d\tau\, dx \tag{3.1}$$

Here b is the background contribution to the measurements at the receptor location, $F(x,\tau;x_s,t)$ is the footprint associated with the current time t and location x_r going back to time $\tau < t$ and location x and $E(x,\tau)$ is the CH_4 emission flux at (x,t). The contributions from emission fluxes are agrregated through a spatio-temporal convolution with the footprints, in Eq. (3.1). The time interval Δt and surface area $\mathbb{A}$ are chosen to reflect all relevant contributions to the $y(x_r,t)$, i.e. emissions outside $\mathbb{A}$ or before $t-\Delta t$ have negligible impact to the CH_4 concentration at (x_r,t). We found that $\Delta_t = 3\ldots4$ days is sufficient to ensure converged results. We expanded this range to $\Delta_t = 7$days to further guarantee that the time range for the aggregate emissions has negligible impact of the results presented here. The settings for the spatial domain $\mathbb{A}$ are detailed later in this section.

In the remainder of this section we present the modeling assumptions taken to approximate the terms in the right-hand side of Eq. (3.1). We first outline the emission model, followed by a description of the atmospheric transport model lending the footprints, and the algorithm for estimating the background contribution. The probabilistic setting adopted to estimate the parameters of this model is introduced in the next section.

For the current analysis we employ Lagrangian footprints for a duration of $\Delta t = 7$ days prior to each measurement point. The emission field $E(x,\tau)$ can be, in general both space and time dependent. In practice, most emission databases have no time dependency, or at best vary from month to month, e.g. the EDGAR database [10].

3.1. EXPERIMENTAL METHODS

The measurements used in this work were taken in Livermore, CA, approximately 45 miles west of the San Francisco peninsula. Air samples were drawn from 27m above ground level from a tower located adjacent to the mobile laboratory housing the analyzer. Prior to being measured using a Picarro CO_2/CH_4/H_2O analyzer, the sample air was passed through a gas dryer to reduce the sensitivity of the dry methane mixing ratio to water vapor corrections. Calibrations of the gas analyzer were performed at regular, 23-hour, intervals using three reference cylinders of synthetic air that was cross-referenced to WMO/NOAA certified whole-air standards.

3.2. ATMOSPHERIC TRANSPORT MODEL

The inversion methodology employed here uses an adjoint model for the atmospheric transport that is derived from a forward atmospheric simulation. The forward model used here was the Weather Research and Forecasting (WRF) model [21], and the adjoint model was the Stochastic Time Inverted Inverse Lagrangian Transport (STILT) model [14]. We ran version 3.7 of the WRF model with modifications to the output fields needed for STILT [19] using initial and boundary conditions derived from the North American Regional Reanalysis. The simulation domain over portions of the western United States and Pacific Ocean included an outer domain covering (domain 1: -156^o<lon.<-86^o, 18^o < lat. < 59^o), and three inner nested domains (domain 2: -140^o < lon < -111^o, 31.5^o < lat. < 47^o; domain 3: -129.5^o<lon. <-117^o, 34.5^o<lat<43^o; domain 4: -125.5^o<lon.<-121^o, 37.25^o < lat.<40.0^o). The grid cell dimensions of the outer domain were 36 km with inner domains nested at a ratio of 3:1 resulting in resolutions of 12, 4, and 1.333 km, respectively. The vertical structure of the WRF grid had 50 levels for all domains, with the model top at 100 mbar. The radiation physics options used were RRTM for longwave radiation and Goddard scheme for shortwave. We used the MYNN 2.5 level TKE scheme for the boundary layer physics, and for surface physics we used the NOAH Land Surface Model. The WRF runs were initiated at 00 hrs UTC for each day and run for a 30 hour simulation time with the first six hours used only for model spin-up and not in subsequent analyses. The outer domain WRF fields were nudged to the NARR analysis fields. For the purpose of evaluation we also executed a subset of the runs both with and without outer-domain boundary layer nudging.

Measurement footprints were calculated using STILT for every hour of the day with a simulated release of 500 particles that were traced over a 7-day period preceding the measurement analysis time. The footprint grid was output at a spatial resolution of 0.1^o in longitude and latitude.

3.3. PRE-PROCESSING FOOTPRINTS AND SURFACE EMISSIONS

In this study we focus on identifying biases corresponding to land sources while employing background measurements that are well characterized. Specifically, let $\mathscr{S}$ be the set of hourly time stamps corresponding to the aggregated experimental observations. Then, from the ensemble of footprints simulated to match the measurements' time stamps $\mathscr{S}$ we select the ones that originate in a large part over the ocean surface, using the test below

$$\int_{t_i-\Delta t}^{t}\int_{\mathrm{A_{ocean}}} F(x,\tau;x_r,t_i)d\tau dx \Big/ \int_{t_i-\Delta t}^{t}\int_{\mathrm{A_{total}}} F(x,\tau;x_r,t_i)d\tau dx > 1-\alpha \tag{3.2}$$

Here we set $\alpha = 0.2$ and if the test above is satisfied, we then add the experimental observations corresponding to t_i to the set of measurements employed to derive biased in methane emissions.

The following steps are taken to create the emission field E for our study. For the land region outside the state of California, we use the EDGAR v4.3.2 anthropogenic emissions corresponding

to year 2012 (the last year available in this database). No interpolation is needed since the computational grid used for our study, $0.1^\circ \times 0.1^\circ$, is aligned with EDGAR grid. For the grid cells for which the centers fall *inside* the California boundaries we augment the EDGAR anthropogenic emissions with the contributions from natural wetland emissions extracted from the CALGEM Project [2]. Since all relevant footprints exhibit sensitivities dominantly from regions inside California, as it will be demostrated below, it is therefore sufficient to account for natural emissions for this region only. Figure 3-1 shows these emissions in a logarithmic scale, to allow lower intensity emissions but distributed over larger regions to be displayed. As expected, higher anthropogenic emissions are observed in urban areas or in regions where agriculture is dominant, e.g. the Central Valley.

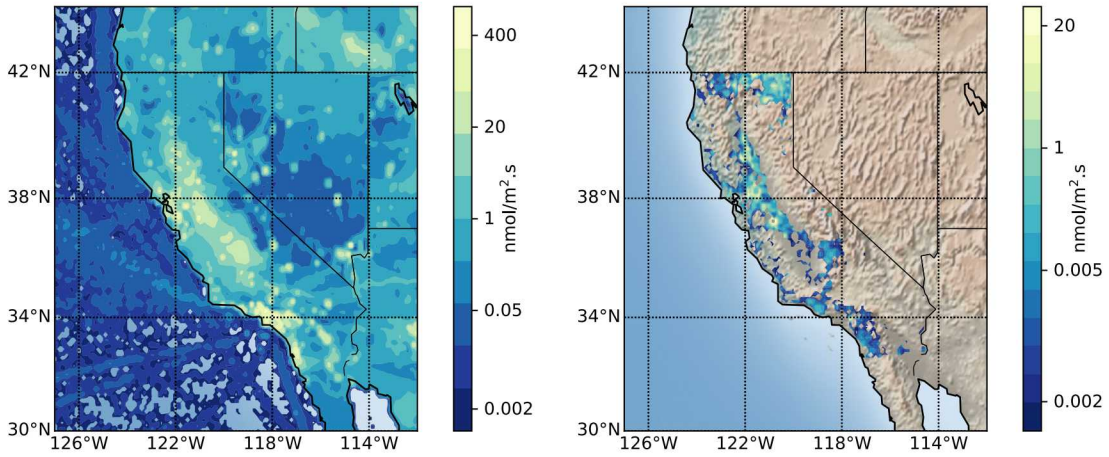

Figure 3-1. EDGAR v4.3.2 anthropogenic emissions (left frame) and CALGEM biogenic emissions (right frame). The concentration levels for both frames are shown in a logarithmic colorscale.

The surface covered by the green patches in Fig. 3-2 indicate grid cells that contributed more than 0.01% to the total model prediction at the Livermore site.

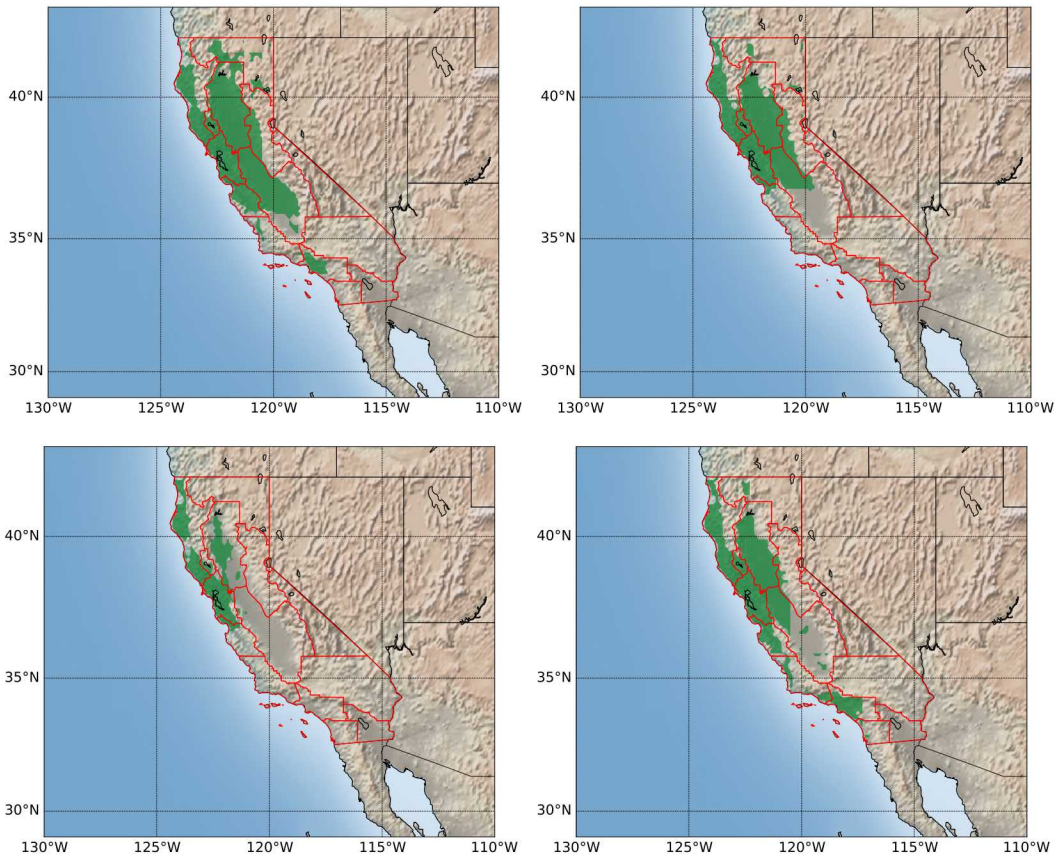

Figure 3-2. Surface area cells marked with green patches contribute at least 0.01% to the total signal (above the background) measured in at the Livermore site. Results correspond to months March to June 2015 (left to right and top to bottom).

4. MODELING BIASES IN EMISSION DATABASES

For the purpose of this work we presume the discrepancy between emission databases and “truth" as far as the spatial distribution is concerned are small. We concentrate our efforts on examining the discrepancy between emission levels and database values given the spatial distribution presented above and assuming it is proportional to the database levels, i.e. a time-dependent multiplicative factor $\lambda(\tau)$

$$E(x,\tau) = \lambda(\tau) E_{db}(x) \tag{4.1}$$

where $E_{db}(x)$ is the database emission (the combination of anthropogenic and biogenic components in Fig. 3-1) at coordinate x, and $\lambda(\tau)$ is the multiplicative bias (or discrepancy) as outlined above. In this expression, we removed the dependency on time for E_{db} since emissions are available on a much coarser time scale, yearly or monthly averages, compared to the measurements' time scale. With this model we expand the integrals in the rhs of Eq. (3.1).

$$\int_{t-\Delta t}^{t}\int_{\mathbb{A}} F(x,\tau;x_r,t)E(x,\tau)d\tau dx = \sum_{i=-(N_t-1)}^{0}\int_{t_{i-1}}^{t_i}\int_{x}\lambda(\tau)F(x,\tau;x_r,t)E_{db}(x)d\tau\, dx \tag{4.2}$$

Here $t_0 = t$ is the current time, $t_i = t - i\delta t$ where $\delta t = 1$day is the time resolution of the footprint data, and $N_t = 7$: $\Delta t = N_t \delta t$. The footprint is usually averaged over each time interval $\overline{F_t(x,\tau;x_r,t)} = F^{(i)}(x,t)$ for $\tau \in (t_{i-1}, t_i)$. The dependency on x_r will be henceforth dropped from the notation since we consider one receptor in this study. With these assumptions the spatial and temporal integrals above can be computed separately

$$\int_{t_{i-1}}^{t_i}\int_{x}\lambda(\tau)F_t(x,\tau)E_{db}(x)d\tau dx = \int_{t_{i-1}}^{t_i}\lambda(\tau)d\tau\int_{x}F^{(i)}(x,t)E_{db}^{(i)}(x)dx \tag{4.3}$$

We now focus our discussion on the modeling of $\lambda(t)$. Current studies employ estimate these biases as constants over select time ranges, e.g. over calendar months or seasons [4, 11]. Here, we expand this model to include a stochastic component for $\lambda(t)$.

4.1. MODELING BIAS AS STOCHASTIC RANDOM FIELD

Generally, a random field/stochastic process is a function that depends on both random and deterministic inputs. Thus, in the present context, the emission bias is modeled as random

function of time. More formally, in a one-dimensional setting consider a bounded domain $D \subseteq \mathbb{R}$ and the sample space Ω, then a stochastic process λ, defined as the mapping $\lambda : D \times \Omega \to \mathbb{R}$, is essentially an infinite collection of random variables $\lambda(t)$, with $t \in D$. Further, we assume that $\lambda(t)$ have finite variance.

The stochastic process λ is centered if the expectation $E[\lambda(t)] = 0$ for all $t \in D$. If λ is not centered, then one can always subtract the expectation $\lambda_0(t) = \lambda(t) - E[\lambda(t)]$ and follow the derivations below for the resulting centered stochastic process. The autocorrelation function C of the stochastic process λ is defined as

$$C(t,s) = E[\lambda(t)\lambda(s)], \quad \forall t,s \in D.$$

It can be shown [13] that C admits the spectral decomposition

$$C(t,s) = \sum_{k=1}^{\infty} \beta_k g_k(t) g_k(s) \tag{4.4}$$

with eigenvalues β_k and eigenfunctions g_k.

The Karhunen-Loeve expansion [5, 16] (KLE) for the stochastic process $\lambda(t,\omega)$ is given by

$$\lambda(t,\omega) = \lambda_0(t) + \theta \sum_{k=1}^{\infty} c_k(\omega) \sqrt{\beta_k} g_k(t) \tag{4.5}$$

where the random variables $c_k(\omega)$ have zero mean, unit variance, and are mutually uncorrelated, $E[c_k c_j] = \delta_{kj}$. Further, if λ is a Gaussian process, then c_k are normal random variables and hence independent. In general, when c_k are non-standard, and their distributions can be inferred from data when available. The KLE representation is *optimal*, corresponding to minimal least-squares error among all possible choices for stochastic fields representation.

In this paper we consider KLE models for temporal Gaussian processes, constructed using a square exponential correlation functions given by $C(t,s) = \exp(-(t-s)^2/l_c^2)$, where l_c is the temporal correlation length. One-dimensional stochastic process realizations for $D = [0,37]$ days are presented in Fig. 4-1 for correlation lengths of half a day and one day, respectively.

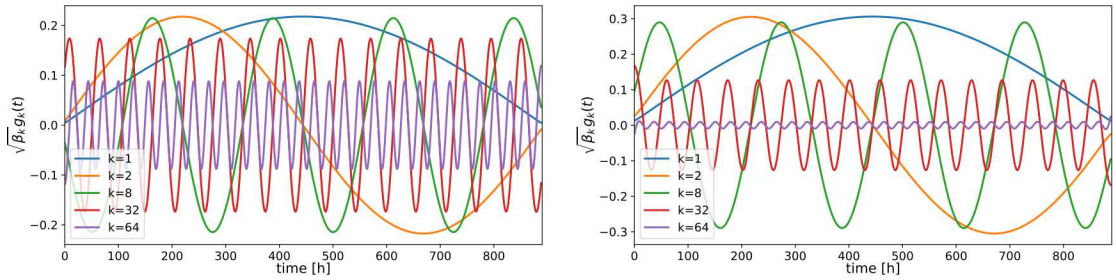

Figure 4-1. Sample scaled KLE modes corresponding to $l_c = 12$h (left frame) and $l_c = 24$h (right frame).

To simplify notation, we absorb the eigenvalue β_k in into the temporal mode, $\sqrt{\beta_k} g_k(t) \to g_k(t)$.

Given the KLE for the bias $\lambda(t)$, the time integral is computed as

$$\int_{t_{i-1}}^{t_i} \lambda(\tau)d\tau = \left(\lambda_0 + \sum_k c_k \frac{1}{\delta t}\int_{t_{i-1}}^{t_i} g_k(\tau)d\tau\right)\delta t = \left(\lambda_0 + \sum_k c_k G_k(t_i,\delta t)\right)\delta t \tag{4.6}$$

where $G_k(t_i,\delta t) = (\int_{t_{i-1}}^{t_i} g_k(\tau)d\tau)/\delta t$ is the average of mode g_k over (t_{i-1},t_i). The spatial integral above is discretized as

$$\int_x F_{t,i}(x)E_{db}(x)dx = \sum_j F_{t,i}(x_j)E_{db}(x_j)\delta x_j \tag{4.7}$$

where the spatial sum is over all surface cells x_j in the computational domain around the point of interest, and δx_j is the area of cell j. Combining Eqs. (4.6) and (4.7) into Eq. 4.2 we get

$$\int_{t-\Delta t}^{t}\int_x F_t(x,\tau)E(x,\tau)d\tau dx = \sum_{i=-(N_t-1)}^{0}\left(\lambda_0 + \sum_k c_k G_k(t_i,\delta t)\right)\sum_j F_{t,i}(x_j)E_{db}(x_j) \tag{4.8}$$

Using the expression in Eq. (3.1), the time dependent concentration generated by the emission model is written as

$$y(t) = b(t) + \sum_{i=-(N_t-1)}^{0}\left(\lambda_0 + \sum_{k=1}^{N_{KLE}} c_k G_k(t_i,\delta t)\right)\sum_j F_{t,i}(x_j)E_{db}(x_j) \tag{4.9}$$

Here, we limited the theoreticaly infinite sum over the KLE modes to, in practice, a finite sum. The number of terms in the sum, N_{KLE}, will be varied to assess the its impact on the quality of the KLE approximation.

4.2. HIERARCHICAL BAYESIAN INFERENCE OF BIAS PARAMETERS

We model the discrepancy between the experimental observations and the model presented above as

$$\mathscr{D} = \boldsymbol{y} + \boldsymbol{\varepsilon} \tag{4.10}$$

Here $\mathscr{D}$ is the vector of hourly concentrations measured over a time span, $\mathscr{D} = \{d_1, d_2, \ldots, d_m\}$, with m the number of measurements. The error term is the sum of contributions due to experimental errors and any discrepancy arising from model inadequacy.

We adopt a hierarchical Bayesian approach to infer the temporal variations in the multiplicative bias in the emission database

$$p(\underbrace{\lambda_0, c_1, \ldots, c_L, \sigma_a, \sigma_m, l_c, b}_{\boldsymbol{\theta}}, \underbrace{\nu, \mu_\lambda, \sigma_\lambda}_{\boldsymbol{\phi}} | \mathscr{D}) \propto p(\mathscr{D}|\boldsymbol{\theta})p(\boldsymbol{\theta}|\boldsymbol{\phi})p(\boldsymbol{\phi}) \tag{4.11}$$

where $\boldsymbol{\theta}$ and $\boldsymbol{\phi}$ are vectors of parameters and hyperparameters, defined as following. The components of the parameter vector $\boldsymbol{\theta}$ are

- $\{\lambda_0, c_1, \ldots, c_L\}$ - the mean and coefficients of the Karhunen-Loéve expansion model of the bias $\lambda(t)$ in Eq. (**??**).
- σ_a and σ_m - additive and multiplicative components defining the covariance model for the model inadequacy, defined below
- l_c - correlation length for the covariance of the Karhunen-Loéve expansion in Eq. (**??**) and the covariance model for the discrepancy between the model and the data.
- b - background for CH_4 concentrations, assumed constant over the time range of the inference

while the components of the hyperparameter vector $\boldsymbol{\phi}$ are given by

- v - the variance of the marginal Gaussian priors for the KLE coefficients
- $\{\mu_\lambda, \sigma_\lambda\}$ - mean and standard deviation for the Gaussian prior for the bias mean λ_0

We model the discrepancy ε between the experimental observations and the model as a multivariate Gaussian with a covariance matrix that accounts for both experimental errors and emission model inadequacies

$$p(\mathscr{D}|\boldsymbol{\theta}) \sim \mathscr{N}(\mathbf{y}, \Sigma) \tag{4.12}$$

The model inadequacy component of the covariance matrix elements is modeled using an exponential decay [11]

$$\Sigma_{i,j} = \Sigma^{(m)}_{i,j} + \delta_{ij}\sigma^2_{e,i},\ \Sigma^{(m)}_{i,j} = \sigma_i \sigma_j \exp\left(-\frac{|t_i - t_j|}{l_c}\right) \tag{4.13}$$

with standard deviation at time t_i modeled as $\sigma_i = \sigma_a + \sigma_m \times y_i$. The correlation length for the decay is l_c, δ_{ij} is the Kronecker delta and $\sigma_{e,i}$ is the experimental error at time t_i.

We consider the conditional independence between model components and a hierarchical approach to write the prior $p(\boldsymbol{\theta}, \boldsymbol{\phi})$

$$p(\boldsymbol{\theta}, \boldsymbol{\phi}) = p(\underbrace{\lambda_0, c_1, \ldots, c_L}_{\boldsymbol{\theta}}, \underbrace{\sigma_a, \sigma_m, \mu_\lambda, \sigma_\lambda, l_c, b, v}_{\boldsymbol{\phi}}) = p(\lambda_0, \mu_\lambda, \sigma_\lambda) \times p(c_1, \ldots, c_L, v) p(l_c) p(b) \tag{4.14}$$

For the mean term λ_0 and hyperparameters μ_λ and σ_λ, the joint prior $p(\lambda_0, \mu_\lambda, \sigma_\lambda)$ is expanded as

$$p(\lambda_0, \mu_\lambda, \sigma_\lambda) = p(\lambda_0|\mu_\lambda, \sigma_\lambda) p(\mu_\lambda) p(\sigma_\lambda) \tag{4.15}$$

with $\lambda_0|\mu_\lambda, \sigma_\lambda \sim \mathscr{N}(\mu_\lambda, \sigma_\lambda)$, $\mu_\lambda \sim \mathscr{N}(1, 0.5)$, $\sigma_\lambda \sim \text{Cauchy}(0, 1)$, and $\lambda_0, \mu_\lambda, \sigma_\lambda > 0$:

$$p(\lambda_0|\mu_\lambda, \sigma_\lambda) \propto \frac{1}{\sqrt{2\pi\sigma^2_\lambda}} \exp\left(-\frac{(\lambda_0 - \mu_\lambda)^2}{2\sigma^2_\lambda}\right),\ p(\mu_\lambda) \propto \frac{1}{\sqrt{2\pi \times 0.5^2}} \exp\left(-\frac{(\mu_\lambda - 1)^2}{2 \times 0.5^2}\right) \tag{4.16}$$

$$p(\sigma_\lambda) \propto \frac{1}{\pi(1 + \sigma^2_\lambda)}$$

During the inference process, normalization constants are computed for the above densities to account for truncation at 0.

The KLE model parameters are a-priori zero-mean uncorrelated. We further assume a Gaussian random field leading to independent conditional priors.

$$p(c_1,\ldots,c_L,v) = p(c_1,\ldots,c_L|v)p(v) = p(v)\prod_{i=1}^{L} p(c_i|v),\ \ p(c_i|v) = \frac{1}{\sqrt{2\pi v}}\exp\left(-\frac{c_i^2}{2v}\right) \tag{4.17}$$

We employ a conjugate Gamma hyperprior for the variance v

$$p(v) = \frac{\beta^\alpha}{\Gamma(\alpha)} v^{-\alpha-1}\exp\left(-\beta/v\right) \tag{4.18}$$

with shape and scale parameters $\alpha = \beta = 1$. The adopt an exponential distribution [11] for the correlation length l_c prior

$$p(l_c) = \frac{1}{l_{c,s}}\exp(-l_c/l_{c,s}) \tag{4.19}$$

with scale $l_{c,s}$ set to 7 days - a typical synoptic time scale for transport [4]. Finally, inspection for the background b indicates we can assumed a Gaussian prior with mean μ_b and standard deviation σ_b based on recorded data for the time range of the inference

$$p(b) = \frac{1}{\sqrt{2\pi\sigma_b^2}}\exp\left(-\frac{(b-\mu_b)^2}{2\sigma_b^2}\right) \tag{4.20}$$

4.2.1. Efficient sampling of $p(\theta,\phi|\mathscr{D})$

A Markov Chain Monte Carlo (MCMC) algorithm is used to construct samples drawn from the posterior distribution $p(\boldsymbol{\theta},\boldsymbol{\phi}|\mathscr{D})$ given in Eq. (4.11). MCMC is a class of techniques that allows sampling from a probability density by constructing a Markov Chain that has the target density as its stationary distribution [3, 6]. In particular, we employ an adaptive Metropolis algorithm ([8]), which uses the covariance of the previously visited chain states to find better proposal distributions, allowing it to explore the posterior distribution in an efficient manner. Nevertheless the adaptive procedure is challenged by the dimensionality of the parameter space, typically resulting in a larger number of samples as the dimensionality of the sampled space increases.

We employ the Raftery-Lewis diagnostic [20] to determine when the Markov Chain converges to stationary posterior distributions. As the chain progresses we asses whether the number of samples drawn so far are sufficient to predict the 5%, 50%, and 95% quantiles of all parameters to within $\pm 1\%$ accuracy with 95% probability. In parallel we also compute the Effective Sample Size [12] (ESS) and aim for values around $10,000$ samples for each parameter. For the set of simulations presented in this paper these convergence test lead to chains with $o(10^6\ldots10^7)$ samples depending on the chain dimensionality. The computation of each sample is described below.

First, the evaluation of the emission model in Eq. (4.9) requires the solution for the eigenvalue problem in Eq. (4.4) for a specific value of the correlation length l_c. The eigenvalue decomposition results in a set of modes $g_k(t)$ which are then integrated over a time span, typically

7 days, ending at the time stamp of each measurement. This renders the direct solution approach all but intractable given that typically sampling approaches require between $o(10^5 \dots 10^7)$ samples and each samples require the integral of each Karhunen-Loeve mode for all measurements' time stamps - between 100-200 for each month.

To circumvent this computational bottleneck we precompute look-up tables for G_k terms that appear in Eq. (4.9) using the steps below

- Solve a set of eigenvalue problems for a range of correlation lengths that is sufficient to cover its posterior distribution. Based on prior experience we constructed a sets of eigenmodes for $l_c \in \{6,8,\dots,20\} \cup \{24,30,\dots,60\} \cup \{72,96,120,168\}$
- For each set of eigenmodes, construct $G_k(t_i, \delta t)$ for each measurement time stamp. Here δt represents the averaging window for each footprint. For the cases presented here $\delta t \approx 1 day$.
- During the sampling step once a specific value for l_c becomes available, the model for the predicted concentrations $y(t)$ is interpolated linearly given the precomputed lookup tables.

5. RESULTS

We conducted two series of numerical experiments. In the first series we constructed a database of methane emissions relying primarily on the EDGAR database [10] for both inside California, as well as outside - over ocean and land areas. Since EDGAR does not include biogenic emissions, we augmented the EDGAR emissions for California with the wetland component from CALGEM [2]. In the second seies of experiments we employed the CALGEM emission fluxes for California. Similar to the previous set of experiments EDGAR information was used for ocean and land areas outside California.

For both series of experiments we conducted a parametric study over the number of modes N_{KLE} in the Karhunen-Loeve expansion for the emission bias. The following sequence was employed, in addition to a baseline case with emission bias constant in time.

$$N_{KLE} = \{12, 18, \ldots, 48\} \cup \{64\}$$

Figure 5-1 shows a typical MCMC output for components of the parameter vector $\boldsymbol{\theta}$ and hyperparamter vector $\boldsymbol{\phi}$. The results in this figure correspond a simulation using EDGAR with $N_{KLE} = 30$. As mentioned above tests using ESS and the Raftery-Lewis diagnostic [20] lead to chain lengths with $10^6 \ldots 2 \times 10^7$ samples.

The MCMC samples were then used to for a statistical analysis of the bias model. First, we constructed marginal densities for the model paramters to gauge their distributions and correlations induced by the experimental data. Figure 5-2 shows 1D and 2D joint posterior distributions for an EDGAR-based simulation with $N_{KLE} = 30$. The results in this figure correspond to a subset of model paramters, specifically the first 12 Karhunen-Loeve modes $c_1, c_2, \ldots, c_{12}$. Strong correlations can be observed between select parameter pairs, suggesting that UQ analyses need to account for these correlations when selecting samples to compute statistics on output quantities of interest.

Next we employed Bayes evidence to select the appropriate parsimony for the bias model represented as a stochastic random field. The Bayes evidence is given by

$$p(\mathscr{D}) = \int p(\mathscr{D}|\boldsymbol{\theta}, \boldsymbol{\phi}) p(\boldsymbol{\theta}, \boldsymbol{\phi}) \, d\boldsymbol{\theta} \, d\boldsymbol{\phi} \tag{5.1}$$

which represents the normalizing factor for the right-hand side of Eq. (4.11) transforming the proportional sign into an equality. We implemented the algorithm proposed by Chib and Jeliazkov [1] to estimate the above integral numerically.

Figure 5-3 shows $p(\mathscr{D})$ in logarithmic scale on the vertical axis as a function of the number of modes in the stochastic random field representation for the bias model. These results,

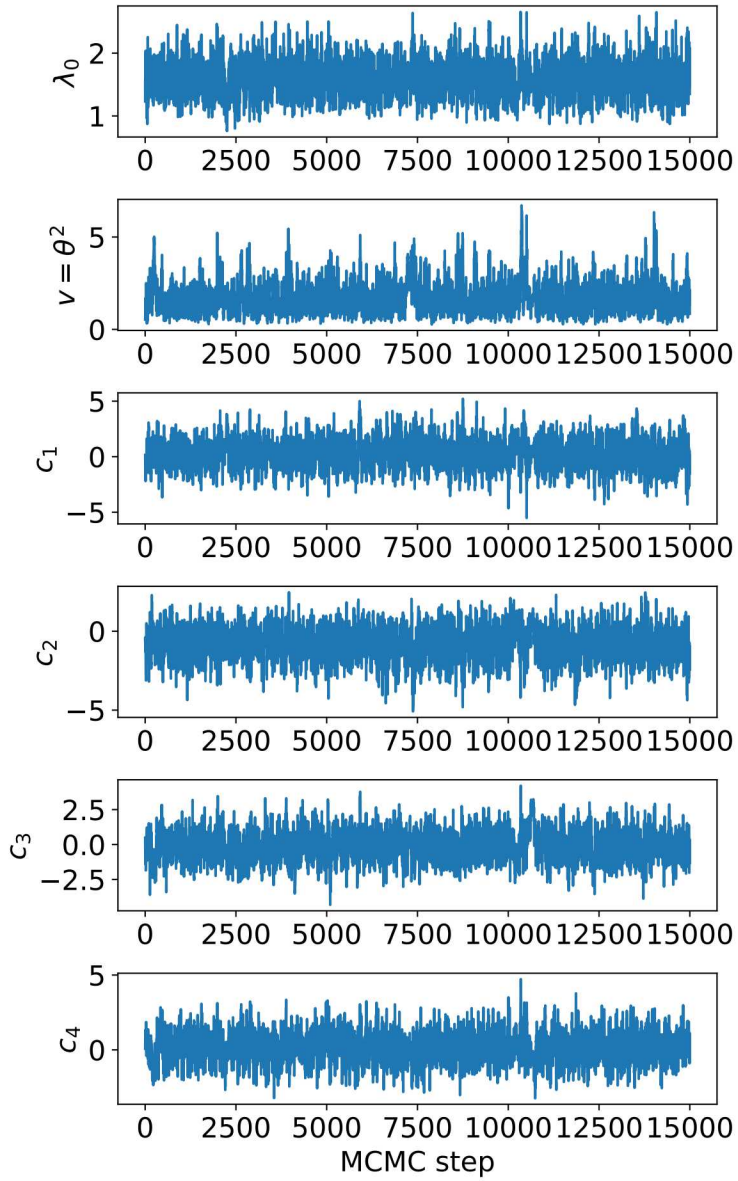

Figure 5-1. Sample chain samples for select variables.

corresponding to numerical experiments employing the EDGAR emissions, indicate that for all sets of tests reported here, the bias model with $N_{KLE} = 48$ exhibits the largest Bayes evidence. Given the discrete set of choices, i.e. simulations with $N_{KLE} = 42$, 48, and 64, the exact optimum could occur for a number of modes slightly off 48. Nevertheless, this refinement level is sufficient to answer the questions addressed in this report.

Using $N_{KLE} = 48$ we investigate statistics on the agreegated bias $\lambda(t)$. The results in Fig. 5-4 show the pushed forward distribution for the bias model $\lambda(t)|p(\boldsymbol{\theta}, \boldsymbol{\phi}|\mathscr{D})$. The shaded green bands correspond to constant quantile leves along the time axis, with dark green indicating values around the mode of the distribution. These results indicate significant temporal variations for the

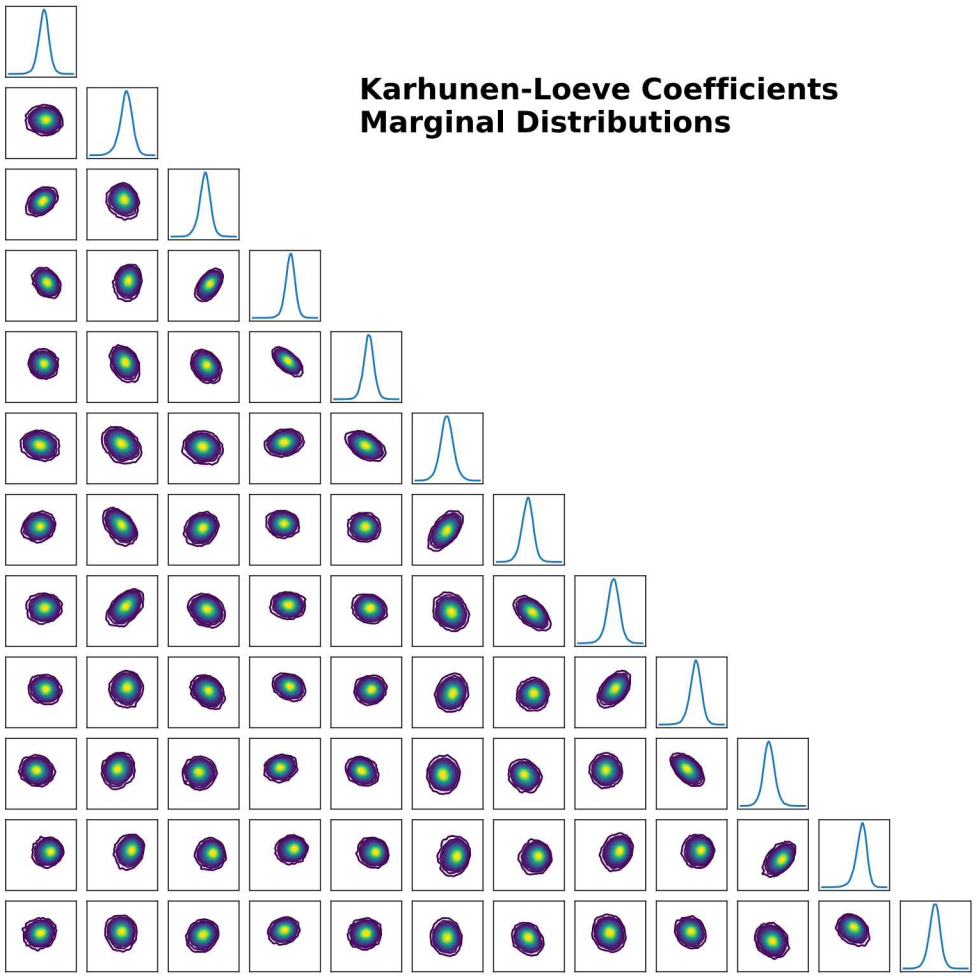

Figure 5-2. 1D and 2D marginals distributions for the first 12 **Karhunen-Loeve coefficients** c_k **corresponding to Run AAA.**

set of simulations that displayed the highest Bayes evidence. Results corresponding to constant bias models are shown with yellow to red color bands.

Next we explore whether the predictive skill of the emission model given the approach presented in Section 4.1. First, we employ the Bayesian posterior predictive distribution ([15]) and examine how well it overlaps with the experimental data. The posterior distribution for the *predicted* data, $p(\mathscr{D}^{(p)}|\mathscr{D})$, is computed by marginalization of the likelihood over the posterior distribution of model parameters and hyperparameters.

$$p(\mathscr{D}^{(p)}|\mathscr{D}) = \int_{\boldsymbol{\theta},\boldsymbol{\phi}} p(\mathscr{D}^{(p)}|\boldsymbol{\theta},\boldsymbol{\phi}) p(\boldsymbol{\theta},\boldsymbol{\phi}|\mathscr{D}) d\boldsymbol{\theta}\, d\boldsymbol{\phi} \tag{5.2}$$

The results presented in Fig. 5-5 indicate a posterior that generally shrinks for the time-dependent model bias compared to the classical approach using constant bias.

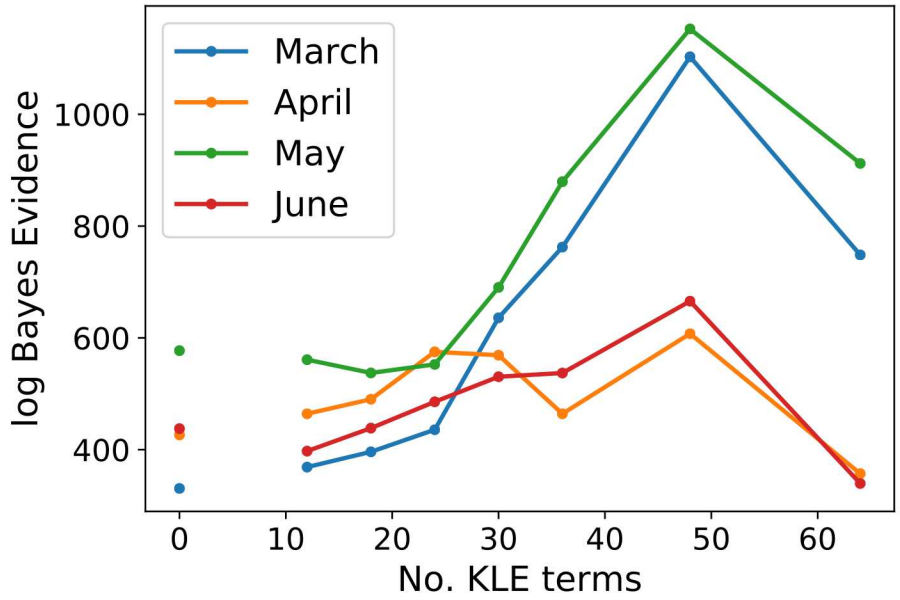

Figure 5-3. Bayesian model evidence computed for models employing a range of Karhunen-Loeve modes.

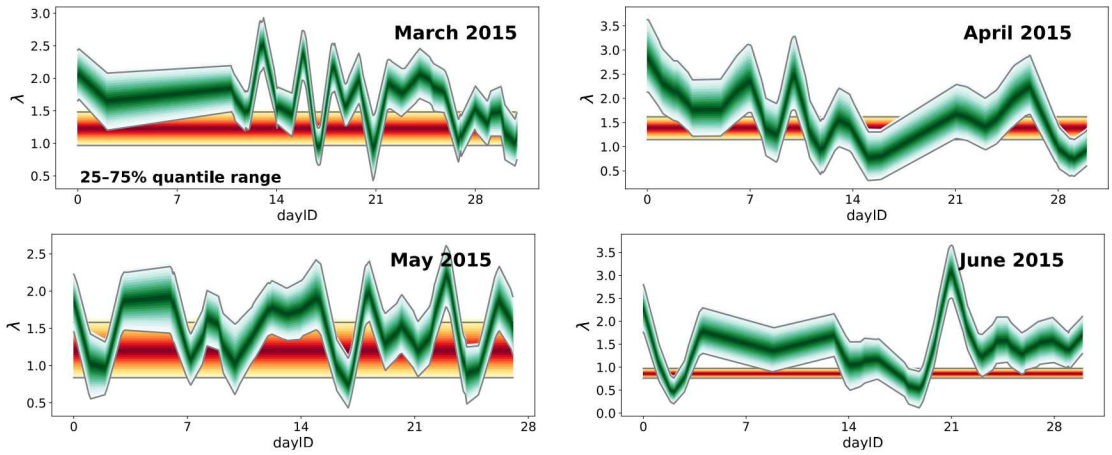

Figure 5-4. Pushed-forward distributions for the time dependent bias $\lambda(t)$.

To quantify the predictive capability of the emission bias model with increasing number of KLE modes, we employ the posterior predictive results above to compute the Continuous Rank Predictive Score (CRPS) [7]. CRPS is an average of the difference between the CDF of the CH_4 observations and the CDF of the predicted data.

$$CRPS(\mathscr{F},\mathscr{D}) = \frac{1}{N_d}\sum_{k=1}^{N_d}\int_{-\infty}^{\infty}\left(\mathscr{F}_k(y_k|\mathscr{D}) - \mathscr{H}_{\mathscr{D}_k}(y_k)\right)^2 dy_k \tag{5.3}$$

Here, $\mathscr{F}_k(y_k|\mathscr{D})$ is the 1D marginal posterior predictive CDF for day k computed using the distributions presented in Fig. 5-5.

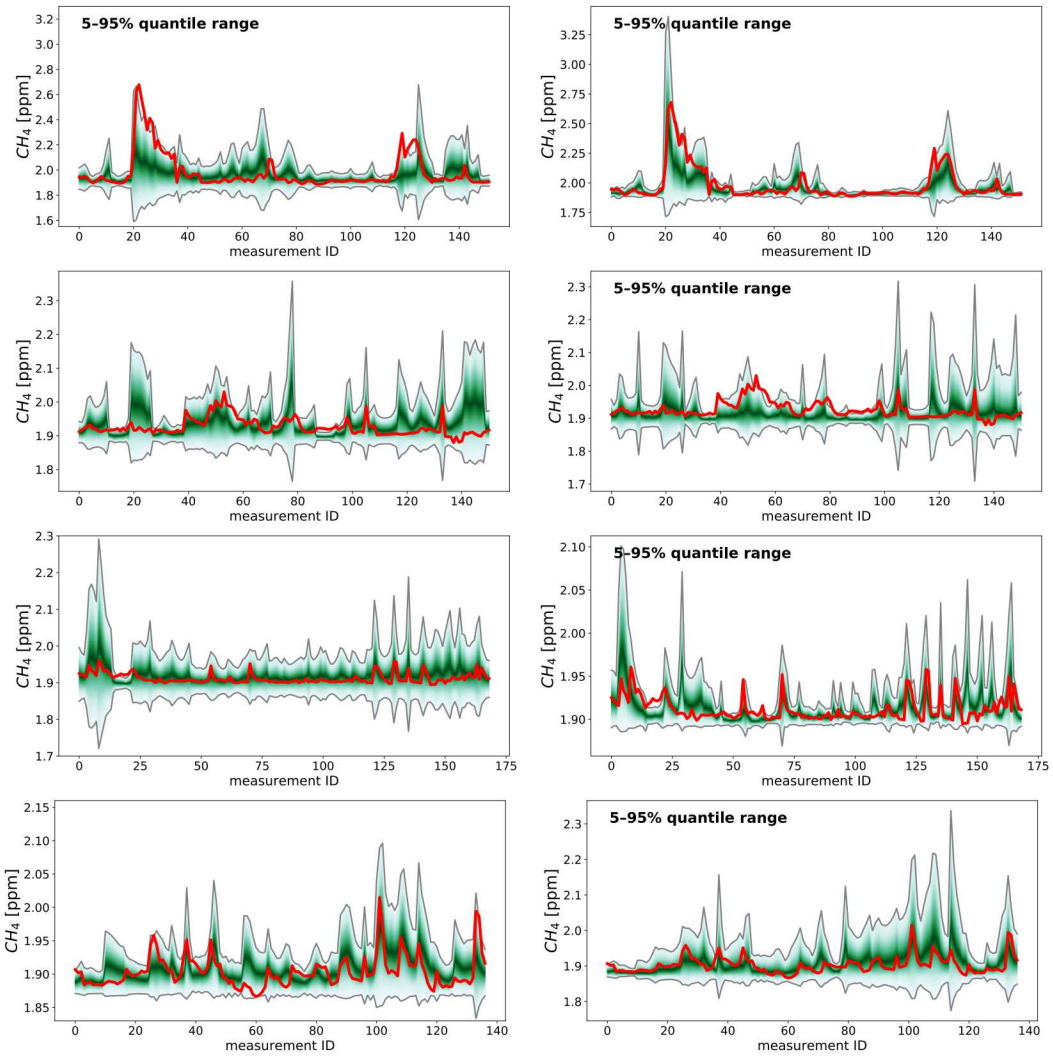

Figure 5-5. Posterior-predictive distribution for the mixing ratios shown with green color bands. Experimental data is shown in red. The left column corresponds to a constant bias model while the right column shows results obtained with 48 Karhunen-Loeve modes. Results on each row (top to bottom) correspond to March, April, May, and June 2015, respectively.

The CDF of the provided data is approximated as a Heaviside function centered at the observation value $\mathscr{D}_k$ citeHersbach:2000, $\mathscr{H}_{\mathscr{D}_k}(y_k) = \mathbb{1}_{y_k \geq \mathscr{D}_k}$.

The CRPS results, shown in Fig. 5-6 corresponding to experiments using CALGEM methane fluxes are lower for all months except March. This indicates a smaller discrepancy between model predictions and experimental observations. Some noise is observed between adjacent points in the horizontal direction. This is likely due to limited number of Markov Chain samples. Nevertheless there is an overall downward trend idicating improved agreement between models and data as more stochastic random field modes are added to the model.

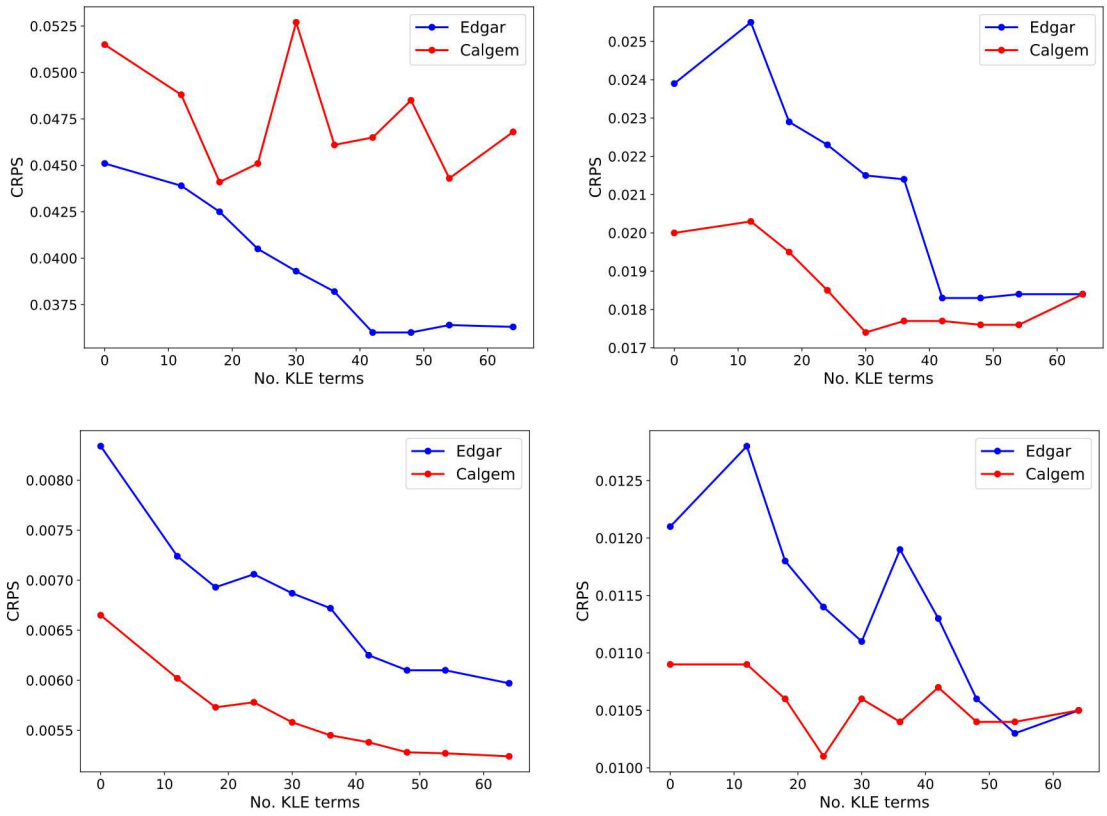

Figure 5-6. Cumulative Rank Predictive Score (CRPS) as a function of the number of Karhunen-Loeve modes. Results correspond to months March to June (left to right and top to bottom).

6. CONCLUSIONS

We present the development and application of a method for trace gas inversion using Bayesian methodology that explicitly accounts for time variation in the model bias. We demonstrate this methodology using methane measurements made in Livermore, California and emissions priors taken from two inventories. We show that the inclusion of the time varying bias can improve the continuous rank probability score and the Bayesian model evidence for the model. We also show that the inferred bias for different emissions sectors can have different temporal structures. For instance we demonstrate that landfills in the the San Francisco Bay area are a minor contributor to the time variation in the estimated bias in the methane emissions by comparison to the non-landfill component.

REFERENCES

[1] Siddhartha Chib and Ivan Jeliazkov. Marginal Likelihood From the MetropolisâĂŞHastings Output. *Journal of the American Statistical Association*, 96(453):270–281, 2001.

[2] M. Fischer, C. Zhao, W. Riley, and A. Andrews. The California Greenhouse Gas Emission Measurements Project. `http://calgem.lbl.gov`. Accessed: 2017-01-30.

[3] Dani Gamerman. *Markov Chain Monte Carlo: Stochastic Simulation for Bayesian Inference*. Chapman & Hall, London, 1997.

[4] A. L. Ganesan, M. Rigby, A. Zammit-Mangion, A. J. Manning, R. G. Prinn, P. J. Fraser, C. M. Harth, K.-R. Kim, P. B. Krummel, S. Li, J. Mühle, S. J. O'Doherty, S. Park, P. K. Salameh, L. P. Steele, and R. F. Weiss. Characterization of uncertainties in atmospheric trace gas inversions using hierarchical bayesian methods. *Atmospheric Chemistry and Physics*, 14(8):3855–3864, 2014.

[5] R.G. Ghanem and P.D. Spanos. *Stochastic Finite Elements: A Spectral Approach*. Springer Verlag, New York, 1991.

[6] W. R. Gilks, S. Richardson, and D. J. Spiegelhalter. *Markov Chain Monte Carlo in Practice*. Chapman & Hall, London, 1996.

[7] T. Gneiting and A. E. Raftery. Strictly proper scoring rules, prediction, and estimation. *Journal of the American Statistical Association*, 102:359–378, 2007.

[8] H. Haario, E. Saksman, and J. Tamminen. An adaptive Metropolis algorithm. *Bernoulli*, 7:223–242, 2001.

[9] Ying-Kuang Hsu, Tony VanCuren, Seong Park, Chris Jakober, Jorn Herner, Michael FitzGibbon, Donald R. Blake, and David D. Parrish. Methane emissions inventory verification in southern california. *Atmospheric Environment*, 44(1):1 – 7, 2010.

[10] G. Janssens-Maenhout, M. Crippa, D. Guizzardi, M. Muntean, E. Schaaf, F. Dentener, P. Bergamaschi, V. Pagliari, J. G. J. Olivier, J. A. H. W. Peters, J. A. van Aardenne, S. Monni, U. Doering, and A. M. R Petrescu. EDGAR v4.3.2 Global Atlas of the three major Greenhouse Gas Emissions for the period 1970-2012. *Earth Syst. Sci. Data Discuss.*, 2017.

[11] Seongeun Jeong, Sally Newman, Jingsong Zhang, Arlyn E. Andrews, Laura Bianco, Justin Bagley, Xinguang Cui, Heather Graven, Jooil Kim, Peter Salameh, Brian W. LaFranchi, Chad Priest, Mixtli Campos-Pineda, Elena Novakovskaia, Christopher D. Sloop, Hope A. Michelsen, Ray P. Bambha, Ray F. Weiss, Ralph Keeling, and Marc L. Fischer. Estimating

methane emissions in california's urban and rural regions using multitower observations. *Journal of Geophysical Research: Atmospheres*, 121(21):13,031–13,049, 2016.

[12] R.E. Kass, B.P. Carlin, A. Gelman, and R.M. Neal. Markov chain monte carlo in practice: A roundtable discussion. *The American Statistician*, 52(2):93–100, 1998.

[13] O.P. Le Maître and O.M. Knio. *Spectral Methods for Uncertainty Quantification*. Springer, New York, NY, 2010.

[14] J. C. Lin, C. Gerbig, S. C. Wofsy, A. E. Andrews, B. C. Daube, K. J. Davis, and C. A. Grainger. A near-field tool for simulating the upstream influence of atmospheric observations: The stochastic time-inverted lagrangian transport (stilt) model. *Journal of Geophysical Research: Atmospheres*, 108(D16), 2003.

[15] S.M. Lynch and B. Western. Bayesian posterior predictive checks for complex models. *Sociological Methods and Research*, 32(3):301–335, 2004.

[16] Y. M. Marzouk and H. N. Najm. Dimensionality reduction and polynomial chaos acceleration of Bayesian inference in inverse problems. *Journal of Computational Physics*, 228(6):1862–1902, 2009.

[17] Scot M. Miller, Steven C. Wofsy, Anna M. Michalak, Eric A. Kort, Arlyn E. Andrews, Sebastien C. Biraud, Edward J. Dlugokencky, Janusz Eluszkiewicz, Marc L. Fischer, Greet Janssens-Maenhout, Ben R. Miller, John B. Miller, Stephen A. Montzka, Thomas Nehrkorn, and Colm Sweeney. Anthropogenic emissions of methane in the united states. *Proceedings of the National Academy of Sciences*, 110(50):20018–20022, 2013.

[18] G. Myhre, D. Shindell, F.-M. Bréon, W. Collins, J. Fuglestvedt, J. Huang, D. Koch, J.-F. Lamarque, D. Lee, B. Mendoza, T. Nakajima, A. Robock, G. Stephens, T. Takemura, and H. Zhang. *Anthropogenic and Natural Radiative Forcing, in: Climate Change 2013: The Physical Science Basis. Contribution of Working Group I to the Fifth Assessment Report of the Intergovernmental Panel on Climate Change*, pages 659–740. Cambridge University Press, Cambridge, United Kingdom and New York, NY, USA, 2013.

[19] Thomas Nehrkorn, Janusz Eluszkiewicz, Steven C. Wofsy, John C. Lin, Christoph Gerbig, Marcos Longo, and Saulo Freitas. Coupled weather research and forecasting–stochastic time-inverted lagrangian transport (WRF–STILT) model. *Meteorology and Atmospheric Physics*, 107(1):51–64, Jun 2010.

[20] A.E. Raftery and S. Lewis. How many iterations in the gibbs sampler? In *Bayesian Statistics 4*, pages 763–773. Oxford University Press, 1992.

[21] William C. Skamarock, Joseph B. Klemp, Jimy Dudhia, David O. Gill, Dale M. Barker, Wei Wang, and Jordan G. Powers. A description of the Advanced Research WRF version 3. NCAR TN-475+STR, 2008.

DISTRIBUTION

Hardcopy—Internal

Number of Copies	Name	Org.	Mailstop
1	D. Chavez, LDRD Office	1911	0359

Email—Internal

Name	Org.	Sandia Email Address
CA Technical Library	8551	cateclib@sandia.gov

Sandia National Laboratories is a multimission laboratory managed and operated by National Technology & Engineering Solutions of Sandia LLC, a wholly owned subsidiary of Honeywell International Inc., for the U.S. Department of Energy's National Nuclear Security Administration under contract DE-NA0003525.